




# Spatial and temporal changes in climate extremes over northwestern North America: the influence of internal climate variability and external forcing

Mohammad Hasan Mahmoudi<sup>1</sup> · Mohammad Reza Najafi<sup>1</sup>  · Harsimrenjit Singh<sup>1</sup> · Markus Schnorbus<sup>2</sup>

Received: 20 August 2019 / Accepted: 11 February 2021 / Published online: 10 March 2021  
© The Author(s), under exclusive licence to Springer Nature B.V. part of Springer Nature 2021

## Abstract

Increases in the intensity and frequency of hydroclimatic extremes associated with climate change can cause significant socioeconomic problems. Assessments of projected extremes using only a limited number of general circulation model (GCM) simulations can undermine the capacity to differentiate and communicate the contribution of internal climate variability (ICV) and external forcing and result in an underestimation of associated risks. In this study, we assess the impacts of climate change on extreme temperature and precipitation and quantify the contribution of internal variability over the Columbia, Fraser, Peace and Campbell River basins in northwestern North America (NWN). Seven GCMs that participated in the Coupled Model Intercomparison Project Phase 5 (CMIP5) and a large ensemble of CanESM2 model simulations (50 members) are downscaled to 1/16° spatial resolution using Bias Correction Constructed Analogues with Quantile mapping reordering version 2 (BCCAQ2). Spatial and temporal changes of climate extreme indices, representing the frequency and intensity of extreme temperature and precipitation, are assessed over the historical (1981–2010) and future (2060–2089) periods under the Representative Concentration Pathway (RCP) 8.5. The influence of ICV on the estimated trends of extreme indices is characterised. Overall, both the frequency and intensity of extreme temperature and precipitation events are projected to increase in NWN indicating more severe dry days and wet conditions in the future. High-elevation Rocky and the Coast Mountains are at larger risks of extreme precipitation, while the Columbia basin, which already faces drought issues, is expected to experience severe dry conditions. Internal climate variability plays a significant role, particularly in the trends of precipitation-related indices. The signal to internal noise ratio

---

✉ Mohammad Reza Najafi  
mnajafi7@uwo.ca

<sup>1</sup> Department of Civil and Environmental Engineering, Western University, London, Ontario, Canada

<sup>2</sup> Pacific Climate Impacts Consortium, University of Victoria, Victoria, British Columbia, Canada

analyses suggest that higher elevations experience stronger forcing signals for precipitation-based indices compared to the other regions.

**Keywords** Climate extremes · External forcing · Internal climate variability · Northwestern North America · CLIMDEX · CMIP5 · CanESM2 large ensemble

## 1 Introduction

According to the Fifth Assessment Report of the Intergovernmental Panel on Climate Change (IPCC AR5), the global average surface temperature has increased by  $0.85 \text{ }^{\circ}\text{C} \pm 0.20 \text{ }^{\circ}\text{C}$  during 1880–2012 (Field et al. 2014). Temperature in Canada has increased at twice the rate of global changes from 1948 to 2016 based on *Canada's Changing Climate Report* (Bush and Lemmen 2019). These changes can lead to decreased snow, reduced soil moisture, higher evapotranspiration, rising sea levels, warming oceans and intensified extreme events, among others that can threaten infrastructure and local communities (Wuebbles et al. 2017). While rising temperature can intensify droughts and heat waves, it increases the moisture-holding capacity of the atmosphere, according to the Clausius-Clapeyron relationship, which can intensify rainfall and flooding events (Pal et al. 2004; Singh et al. 2020; Zhang and Najafi 2020). In addition to the anthropogenic effects, the internal processes within the climate system and the interactions between the atmosphere, ocean and land surface components (i.e. internal variability) play a significant role in regional precipitation and temperature variations (Deser et al. 2012; Fischer et al. 2013; Xie et al. 2015). Therefore, to develop effective adaptation and resilience plans, it is critical to assess projected extremes under climate change and characterise the role of internal climate variability (ICV).

Although recent studies have investigated the effects of internal variability on hydroclimate variables (Acero et al. 2011; Dai and Bloecker 2019; Hegerl et al. 2015), assessments of projected extremes are mainly focused on external climate forcing particularly at regional scales. Previous studies have found increases in the frequency and intensity of extreme events in many regions around the world during the second half of the twentieth century (Frich et al. 2002; Kiktev et al. 2003; Najafi et al. 2017a, 2017b; Abbasian et al. 2020a, 2020b). They show stronger heat temperature extremes and decreased cold extremes (Hansen et al. 2006; Orłowsky and Seneviratne 2012), non-uniform patterns of change in precipitation-related extremes (Jalili Pirani and Najafi 2020; Kharin et al. 2007; Orłowsky and Seneviratne 2012) and nonstationary behaviour of temperature and precipitation dependencies (Singh et al. 2021). These trends are projected to continue to increase in the future (Tebaldi et al. 2006; Sillmann and Roeckner 2008; Sillmann et al. 2013).

Regional studies over different parts of NWSA project increases in temperature (Bürger et al. 2013; Murdock et al. 2013; Whan and Zwiers 2016), declines in both maximum Snow Water Equivalent (SWE) (Bürger et al. 2013; Krasting et al. 2013) and summer streamflow (Najafi et al. 2017a, 2017b). Li et al. (2018) showed that western Canada is projected to be warmer and wetter with increased frequency of extreme events. The mean annual temperature and annual total precipitation are projected to increase over key river basins of western Canada including Upper Columbia River Basin (Murdock et al. 2013), Peace River Basin (Andrishak and Hicks 2008) and Fraser River Basin (Morrison et al. 2002).

Internal variability can dominate climate change signals at various temporal scales (Hegerl et al. 2015), and it is important to characterize its role in the trends of climate extremes.

Numerous studies on climate extremes have been conducted based on single realisations from a set of GCMs, which suggest that the multi-model ensemble mean provides a more reliable representation of external climate forcing compared to individual simulations (Bürger et al. 2013; Murdock et al. 2013; Whan and Zwiers 2016). However, distinguishing between the response to external forcing and internal variability is challenging in multi-model ensembles since the underlying signal can be attributed to multiple other factors such as non-linearities arising from the model physics. Furthermore, the uncertainty associated with the spread of the multi-model ensemble represents the effects of internal variability and model structure and cannot be used directly to represent ICV. Single-model ensemble runs, which are generated by driving an individual GCM multiple times with different initial conditions but similar external forcings, provide a direct way to differentiate the two factors. The spread of different runs of the GCM in such a case can only be attributed to the internal variability of the model itself, while the average of all runs represents the external climate forcing (Dai and Bloecker 2019).

To address these research gaps, we quantify the contribution of ICV to climate change impacts on temperature and precipitation extremes at regional scales. Although recent studies have investigated the role of internal variability, however, such analyses at fine scales, in which regional effects can be significant, are rare. We assess the climatic extremes of NWNA at a relatively high spatial resolution ( $1/16^\circ$ ) and quantify the role of internal variability in historical and future trends of climate extremes. Furthermore, we evaluate and compare the uncertainties arising from the CMIP5 multi-model ensemble vs. individual model simulations based on perturbed initial conditions (i.e. CanESM2; 50 members). NWNA has a complex topography with highly heterogeneous river basins in terms of physiography and climatology and high diversity in water usage, which includes major cities such as Vancouver and Seattle. To the knowledge of the authors, this would be the first analysis of internal variability beside the response to external forcing in this region.

The remainder of the paper is organised by describing the study area and data in Section 2. Section 3 discusses the downscaling approach, CLIMDEX indices analysed in this study, and the role of single-model ensemble in internal variability. Section 4 presents the spatial and temporal changes of climate extremes and the role of internal variability over NWNA followed by the conclusions in Section 5.

## 2 Study area and data

The study domain includes four key river basins in NWNA located between the Pacific Ocean on the West and the Rocky and Columbia Mountain Ranges on the East with a total area of 958,000 km<sup>2</sup> (Fig. 1) and a population of more than 14 million (Northcote 1996; 2016 census population and dwelling counts). It has a complex topography and includes parts of British Columbia and Alberta in Canada, and the states of Washington, Oregon, Idaho and Montana in the USA.

The Columbia River is 1954 km long and drains an area of approximately 616,000 km<sup>2</sup>. CRB ranges from 390 to 3700 m in elevation and has a humid continental climate with an average temperature varying between  $-9.2^\circ\text{C}$  in January and  $13.3^\circ\text{C}$  in July. CRB is mainly a snowmelt-driven (nival) system (Pulwarty and Redmond 1997) and has a wide range of average annual precipitation from almost 200 mm over the eastern Rockies, including the Snake River basin, to more than 1500 mm in the coastal mountains. It receives most of its

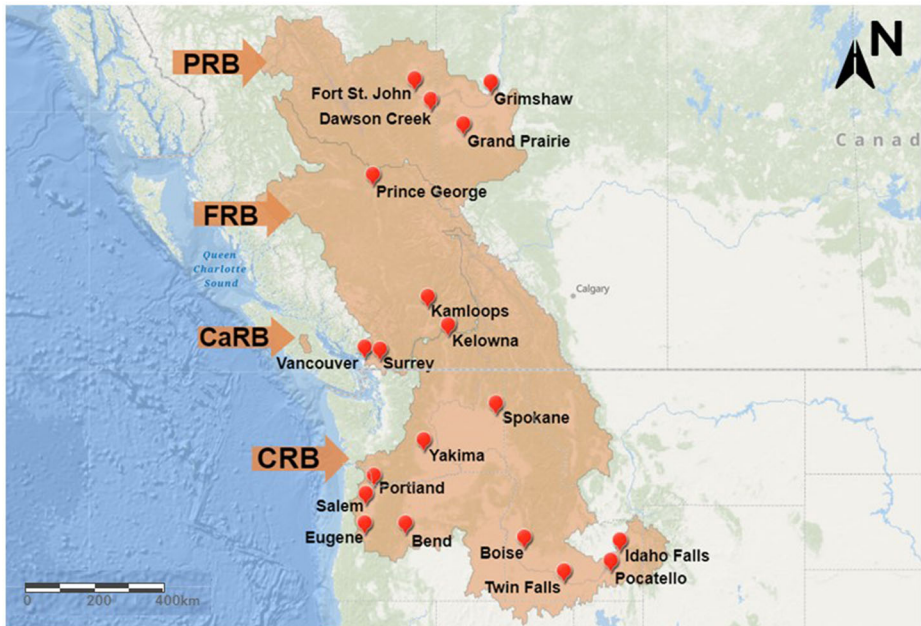


**Fig. 1** Study area including four major river basins in northwest North America

precipitation in winter and the remaining 20% in June to August. The Fraser River Basin (FRB) is one of the largest watersheds in western Canada with a drainage area of 230,000 km<sup>2</sup> that includes densely populated (67% of British Columbia's population) urban areas (including the city of Vancouver) and diverse ecosystems (Shrestha et al. 2012). The elevation ranges from sea level to 4000 m. According to gridded observations derived from Environment and Climate Change Canada's climate station observations, FRB's mean annual temperature and precipitation vary between  $-5$  and  $10$  °C and 200 and 5000 mm, respectively. The Peace River Basin (PRB) is located in Northern British Columbia and extends to Alberta. It covers an area of approximately 101,000 km<sup>2</sup> with elevation ranging from 400 to 2800 m. PRB's average temperature is between  $-11.7$  °C in January and  $12.4$  °C in July and most of the annual precipitation occurs between October–April (Najafi et al. 2017a). The Campbell River Basin (CaRB) in Vancouver Island drains an area of 1193 km<sup>2</sup> with elevation ranging between 139 and 2200 m. It receives a large amount of total annual precipitation of 5716 mm with temperature ranging between  $-4$  and  $16$  °C (Bennett et al. 2012). Although CaRB is relatively small in size compared to the other basins, it is included in these analyses because it has a distinct climate and is close to the Pacific Ocean.

We used the Pacific Climate Impacts Consortium (PCIC) meteorology for NWA (PNWNAme) as the most recent and reliable gridded daily precipitation, maximum temperature and minimum temperature dataset with  $1/16^{\circ}$  resolution for 1951–2010 (Werner et al. 2019). To assess climate change impacts, simulations from seven CMIP5 GCMs (single runs; hereafter SR\_GCM) based on the Representative Concentration Pathway (RCP) 8.5 are used over the historical and future periods of 1981–2010 and 2060–2089, respectively. These models include ACCESS1-0 (Bi et al. 2013), ACCESS1-3 (Bi et al. 2013), CanESM2 (Chylek et al. 2011), CCSM4 (Gent et al. 2011), CNRM-CM5 (Voldoire et al. 2013), HadGEM2-ES (Jones et al. 2011) and MPI-ESM-LR (Giorgetta et al. 2013). In addition, a

large ensemble of 50 climate simulations generated by perturbing the CanESM2 model initial conditions, i.e. CanESM2\_LE, is used to distinguish the uncertainties in model structure and internal variability and better assess the projected changes in regional climate extremes. All GCMs are downscaled using Bias Correction Constructed Analogues with Quantile mapping reordering version 2 (Werner and Cannon 2016).

### 3 Methodology

#### 3.1 Downscaling

We downscale daily precipitation, maximum temperature and minimum temperature from seven GCMs and CanESM2\_LE (50 members) using the Bias Correction Constructed Analogues with Quantile mapping reordering version 2 (BCCAQ2) approach (Werner and Cannon 2016). BCCAQ2 is a hybrid approach that combines bias-correction and climate imprint (BCCI; Hunter et al. 2005) with bias correction constructed analogues (BCCA; Maurer et al. 2010). BCCI calculates daily anomalies of GCM outputs (i.e. temperature and precipitation) based on the monthly climatology at each coarse-scale grid cell. Anomalies are interpolated to fine-scale observed grids and multiplied (for precipitation) or added (for temperature) to the observed monthly climatology. Downscaled GCMs are then bias-corrected using the quantile mapping approach. BCCI preserves the temporal sequence of GCM variability but has poor spatial covariability especially in mountainous regions due to the smoothing process in interpolation. BCCA uses quantile mapping to bias-correct daily coarse-scale GCM outputs (temperature and precipitation) based on coarse-scale observations (Werner et al. 2019). Instead of using a smooth interpolation scheme, BCCA generates fine-scale downscaled patterns by regressing future GCM simulations in each day on a linear combination of best matching (analogue) historical observations (Hidalgo et al. 2008). The method represents the topographic effects; however, it does not capture simulated daily sequencing and tends to produce too much drizzle and underestimate extreme precipitation. BCCAQ2 reorders daily BCCI outputs for each month based on BCCA to improve spatiotemporal variability and uses quantile delta mapping instead of regular quantile mapping to preserve all projected quantiles in the downscaled output. BCCAQ2 retains the advantages of both BCCI and BCCA approaches and better represents extreme events, day-to-day sequencing and spatial covariance. Extensive research has been conducted to evaluate the performance of downscaling approaches and the corresponding uncertainties (Chen et al. 2012; Diaz-Nieto and Wilby 2005; Fauzi et al. 2020; Najafi et al. 2011; Singh and Najafi 2020; Werner and Cannon 2016; Yang et al. 2019). BCCAQ has shown satisfactory performance in replicating historical CLIMDEX indices and hydrological climate change impact assessments (Werner and Cannon 2016). The downscaling and bias-correction process is performed over each GCM ensemble member (57 runs) for the entire NWA. Figure S1 shows the advantage of downscaled GCM simulations to better represent regional variations of hydroclimatic extremes compared to raw GCM outputs.

#### 3.2 CLIMDEX

Twenty-seven climate extreme indices (i.e. CLIMDEX) are defined by the Expert Team on Climate Change Detection and Indices (ETCCDI) based on daily data, from which 16 are

temperature-related and 11 are precipitation-related. Most of these indices represent moderate extremes that occur at least once a year. Some indices can be used to estimate hydroclimatic extremes with long return periods using sufficiently long annual maximum data series. CLIMDEX can be divided into two categories. One that characterises the intensity of climatic extreme events and the other that measures the frequency of extremes exceeding a certain threshold (Zhang et al. 2011). Analysis of both types of indices is critical for the design and planning of structure and infrastructure, agricultural and water resource management. We selected eight indices that best represent the intensity and frequency of extreme temperature and precipitation (Karl et al. 1999; Zhang et al. 2005). These indices are widely used because they can represent the impacts of climate extremes on industries, agriculture, hydropower generation, fishery and forestry activities as well as natural disasters such as droughts, floods and wildfires (Tebaldi et al. 2006; Werner and Cannon 2016). The climate extreme indices used in this study (TXx, TNn, GSL, CDD, RX5day, R10, SDII and R95) are described in the Supplementary information and summarised in Table S1.

### 3.3 Internal variability

Using the large ensemble simulations, we quantify the influence of ICV and external forcings on historical and projected trends. The linear trend of each extreme climate index is estimated using the least-squares method for both historical and future periods. Furthermore, we assess spatial changes of internal variability across the basins over the historical and future periods.

$$IV_{i,T} = V_{i,T} - F_T, \quad (1)$$

The linear trend in the ensemble mean,  $F_T$ , represents the forced response of the system, and the linear trend in the anomaly time series for each ensemble member,  $IV_{i,T}$ , represents that member's internal variability (Dai and Bloecker 2019). In addition, the signal-to-noise ratio (SNR) is calculated to quantify how trends in extreme indices are affected by the underlying noise:

$$\text{SNR} = \frac{\text{Trend}_{\text{EF}}}{(\sum_{i=1}^N \text{SD}_i) / N}, \quad (2)$$

where  $\text{Trend}_{\text{EF}}$  is the trend in extreme index associated with the response to external forcing (ensemble mean),  $\text{SD}_i$  is the standard deviation of ensemble member  $i$  and  $N$  ( $=50$ ) is the total number of ensemble members.

## 4 Results

### 4.1 Spatial patterns of extreme precipitation and temperature over NRNA

The spatial distribution of temperature-based (intensity: TNn, TXx and frequency: GSL) and precipitation-based (intensity: RX5day, SDII, R95 and frequency: CDD, R10) indices is evaluated over NRNA using gridded observations, CanESM2\_LE and SR\_GCM simulations over the historical (1981–2010) and future (2060–2089) periods at a  $1/16^\circ$  spatial resolution. The following sections present the results of TNn, TXx (as representatives of temperature-based indices) CDD and R95 (as representatives of precipitation-based indices). Other indices are presented in the Supplementary information.

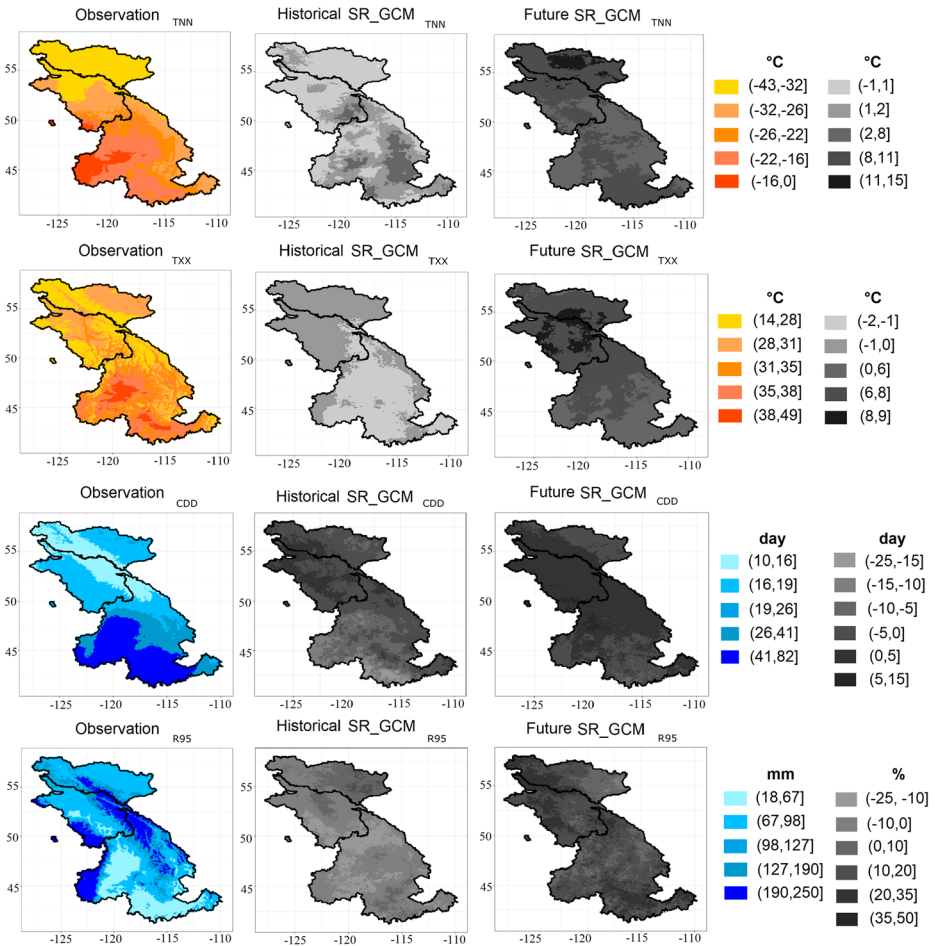


**Fig. 2** Spatial variability of T<sub>nn</sub> (first row), TX<sub>x</sub> (second row), CDD (third row) and R<sub>95</sub> (fourth row) based on gridded observations (left panel), historical biases (middle panel) and future projections (right panel) of SR\_GCM means. Projected distributions of CLIMDEX (right panels) show the changes of CLIMDEX in the future period compared to their historical period over NWNA

Figures 2 and 3 and S2 and S3 show the CLIMDEX indices using gridded observation in colour (left panels of the figures) and the bias of the simulations using SR\_GCMs (Figs. 2 and S2) and CanESM2\_LE (Figs. 3 and S3) for the historical period (middle panels) and their projected changes in the future period (right panels) in grayscale.

### 4.1.1 SR-GCM simulations

CRB particularly the western parts and southern FRB experiences the weakest extreme cold conditions in terms of the average T<sub>nn</sub> among other regions in NWNA, while PRB and northern FRB are the coldest during the late twentieth century (Fig. 2). Furthermore, SR\_GCMs (7 members) overestimate the average T<sub>nn</sub> over high elevation areas (the Rockies in southeastern FRB and eastern CRB) with the highest bias over eastern parts of CRB. SR\_GCMs show relatively good performance in other areas of NWNA. The projected T<sub>nn</sub>

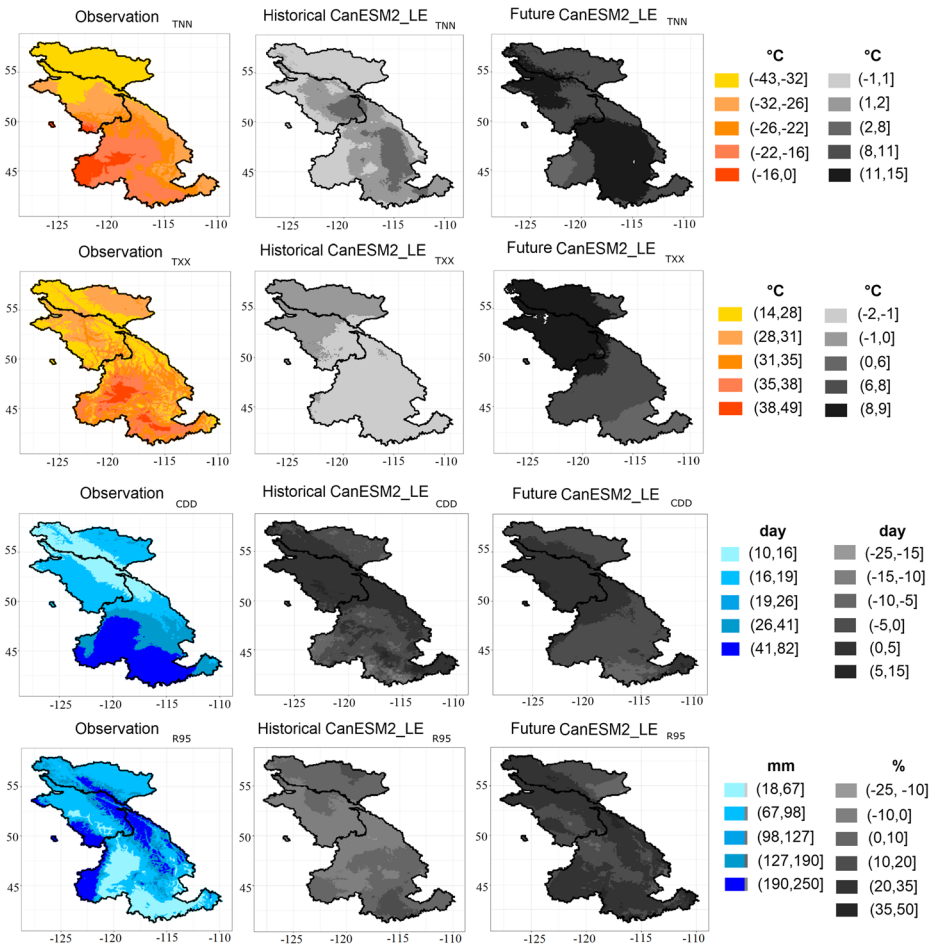


**Fig. 3** Spatial variability of Tn (first row), TXx (second row), CDD (third row) and R95 (fourth row) based on gridded observations (left panel), historical biases (middle panel) and future projections (right panel) of CanESM2-LE means. Projected distributions of CLIMDEX (right panels) show the changes of CLIMDEX in the future period compared to their historical period (middle panels) over NWA

(Fig. 2) shows a notable increase over the entire NWA, with the highest increase up to 15 °C over northern PRB. Tn over major cities of FRB (Vancouver, Surrey, Kelowna and Kamloops) and CRB (Portland, Salem, Eugene, Yakima, Bend and Spokane) is projected to increase between 2 and 8 °C, while over other major cities (FRB: Prince George, PRB: Grande Prairie and Grimshaw, CRB: Twin Falls, Boise, Idaho Falls and Pocatello, entire CaRB), it is projected to increase between 8 and 11 °C.

Central and southern CRB have been the hottest regions of NWA based on observed TXx reaching 38–49 °C (Fig. 2). The lowest TXx over NWA occurs over high elevation regions as well as CaRB ranging between 14 and 28 °C (eastern and western NWA), while Vancouver and Surrey, which are close to high elevation areas, experience between 1 and 2 °C higher TXx that might be due to urban heat island effect. SR\_GCMs slightly underestimate TXx (up to 2 °C) in the same locations where SR\_GCMs overestimate Tn as well as central CRB; however, they show good performance in simulating TXx in other parts of



NWNA. In other words, the downscaled SR\_GCMs are slightly biased in capturing extreme temperatures (minimum and maximum) over central CRB and southeastern FRB. According to the future simulations, NWNA is projected to face a significant increase in the intensity of TXx (averages up to 7 °C) particularly around Prince George and Kamloops with 8–9 °C.

Regions in the south and west of CRB show a higher frequency of CDD (between 41 and 82 days) over the late twentieth century compared to the other parts of NWNA, while the lowest CDD (10–16 days) occurs along eastern FRB and western PRB including the high elevation regions across FRB and PRB (Fig. 2). The SR\_GCM mean underestimates CDD over NWNA, which implies less persistent dry periods in the models compared to the observations. The CDD bias of SR\_GCMs increases in higher latitudes and high elevation regions. CDD is projected to increase over CaRB, entire FRB, upper CRB including Columbia mountains and lower PRB and decrease in parts of southern CRB as well as upper PRB. Most of these areas are also affected by increases in TXx and TNn (temperature-related), which, combined with more frequent CDD (precipitation-related), can experience dramatic hydroclimatic conditions that can cause severe socioeconomic consequences such as agricultural land threats, higher risk of wildfires and more frequent and severe droughts.

Coastal regions in southwestern FRB, western parts of CRB and CaRB, and the mountainous areas including the Upper Rockies and the Columbia Mountains show the highest total precipitation (between 190 and 250 mm) in very wet days (R95; Fig. 2). SR\_GCMs could not represent the observed R95 patterns well and underestimated the averages up to 20% throughout NWNA except in northern FRB and eastern PRB where R95 has been captured well (Fig. 2). Furthermore, the mean of these ensembles project increases over NWMA with the highest increase over high elevation areas of western PRB and FRB including Prince George as well as CaRB (averages between 30 and 50%).

CaRB and major cities such as Vancouver, Surrey, Spokane, Fort St John, Dawson Creek and George Prairie are projected to experience more frequent and severe hot and wet extreme events (Fig. 2). Central and western CRB have the longest growing season length in NWNA. Areas with the lowest TXx values including the upper CRB, along the Columbia Mountains, western PRB and FRB, and CaRB, have shorter GSLs compared to the other regions in NWNA. SR\_GCM captures the observed spatial pattern of this temperature-related extreme index well except southern CRB and northern PRB that GSL has been underestimated up to 20 days. GSL is projected to increase in the future period throughout NWNA with larger increases in southern latitudes particularly over CRB in the USA, compared to the north (Fig. S2). The other precipitation-based indices (R10, Rx5day and R95) are shown in Fig. S2. Their observed spatial patterns are similar to each other such that the most intense wet events occurred in CaRB, southwestern FRB, western parts of CRB, and CaRB, and the mountainous areas including the Upper Rockies and the Columbia Mountains. R10 is projected to increase over NWNA particularly on higher elevations of the Rockies; however, SR\_GCMs slightly underestimate R10 over CRB in the historical period. Due to the high variability of precipitation over mountainous areas, the simulation based on SR\_GCM shows slight underestimations in these regions. More intense RX5day events are projected over the future period mainly along high elevations in western and eastern NWNA. The observed spatial pattern of SDII is well-represented by SR\_GCMs. Also, SR\_GCMs project increases in the average precipitation rate during wet periods (up to 35%) over the entire domain particularly along the upper Rocky Mountains and the Columbia Mountains.

### 4.1.2 CanESM2\_LE simulations

The CanESM2\_LE mean (the average of 50 members) captures TNn well, particularly over high elevation area; however, it slightly overestimates TNn over the Rockies in southeastern FRB and eastern CRB. Furthermore, CanESM2\_LE projects remarkable increases in TNn (up to 15 °C) particularly over western FRB and central and eastern CRB (Fig. 3). Historical TXx is slightly underestimated over CRB but captured well by CanESM2\_LE over the other river basins (Fig. 3). According to CanESM2\_LE projections (Fig. 3), TXx in the entire NRNA is expected to increase notably (averages up to 9 °C). Results indicate that parts of NRNA such as PRB tend to experience relatively smaller increases in extreme cold in the future but larger increases in extreme heat. Contrary to this, central CRB can face larger increases in extreme cold. The entire CaRB and some other major cities such as Vancouver, Surrey, Prince George, Kamloops and Kelowna are projected to experience significantly hot temperatures in the future (between 8 and 9 °C increase in TXx).

CanESM2\_LE shows good performance in simulating CDD over NRNA except for FRB, eastern CRB and western PRB where it underestimates CDD between 10 and 15 days (Fig. 3). The projected spatial distribution of CDD is similar to that of SR\_GCM. CanESM2\_LE captures R95 well (Fig. 3), although R95 over northern CRB and southwestern FRB is slightly underestimated (averages up to 25%). The coastal basin of NRNA shows the highest projected changes of R95 with 35–50% increase.

Spatial distributions of the other indices (GSL, R10, Rx5day and SDII) are shown in Fig. S3. CanESM2\_LE captures the observed spatial pattern of GSL well. This temperature-based index is projected to increase in the future period over the entire NRNA with larger increases in central CRB and well as entire CaRB. The spatial pattern of R10 is similar to that of R95 and CanESM2\_LE shows good performance in simulating R10 in the historical period. R10 is projected to increase (averages up to 30 days) throughout NRNA with larger increases on higher elevations of the Rockies (similarly to SR\_GCMs projections).

Downscaled CanESM2\_LE underestimates RX5day over mountainous areas. RX5day is projected to increase significantly (averages by 50%) in the future period over entire NRNA particularly in mountainous regions as well as CaRB. Similar to other precipitation-based indices that determine the frequency of extreme events, CanESM2\_LE could capture the spatial pattern of precipitation intensity (SDII, showing the intensity of extreme event) well. Furthermore, it projects increase in SDII during wet periods throughout NRNA particularly mountainous regions.

## 4.2 Temporal trends of extreme indices

### 4.2.1 SR\_GCMs annual variations

Temporal variations of all aforementioned indices over NRNA are shown for the historical and future periods using the gridded observation and SR\_GCM simulations (showing the means and 95% uncertainty ranges) (Fig. S6). The average TNn over NRNA is projected to increase notably (almost 8 °C) based on SR\_GCM. The difference between future and historical TXx means is 6.5 °C. The ensemble means of simulated TNn and TXx averaged over the future period exceeds their maximum observed values and the simulated historical 95th percentile. The average CDD is captured well by SR\_GCMs and is projected to slightly increase (1.5 days). The corresponding difference between the future and historical R95

simulations is 17.9 mm. According to SR\_GCMs, temporal projections of spatially averaged GSL, R10, RX5day and SDII are projected to increase in the future period.

### 4.2.2 CanESM2\_LE annual variations

Overall, the temporal variations of extreme indices based on CanESM2\_LE (Fig. 4) are consistent with those of SR-GCMs. The average observed TNn over NWNA is  $-25.1\text{ }^{\circ}\text{C}$ , which is projected to increase to  $-14.9\text{ }^{\circ}\text{C}$  based on CanESM2\_LE (top left panel of Fig. 4). According to CanESM2\_LE, the difference between future and historical TNn ensemble means is  $9.5\text{ }^{\circ}\text{C}$ . Moreover, the average observed TXx value of  $29\text{ }^{\circ}\text{C}$  is projected to increase to  $37.3\text{ }^{\circ}\text{C}$ . The difference between future and historical TXx means is  $7.8\text{ }^{\circ}\text{C}$ . As shown in the bottom left panel of Fig. 4, the average number of observed consecutive dry days is 13 days, which is slightly overestimated based on CanESM2\_LE mean (as 13.5 days). CDD is projected to slightly increase by 0.21 days in the future period according to CanESM2\_LE. The observed R95 value of 100.8 mm is projected to increase to 136.1 based on CanESM2\_LE over the future period (2060–2089). The corresponding difference between the future and historical R95 simulations is 32.8 mm.

Temporal variability of the other indices (GSL, R10, RX5day and SDII) based on CanESM2\_LE is shown in Fig. S7. Overall, the results suggest that the intensity and frequency of temperature-related and precipitation-related extreme indices are projected to increase in NWNA based on both ensembles.

### 4.3 Impact of internal variability on trends

In both historical and future periods, TNn shows a larger trend compared to TXx indicating a larger shift in the lower tail of the temperature distribution as compared to its upper tail. This

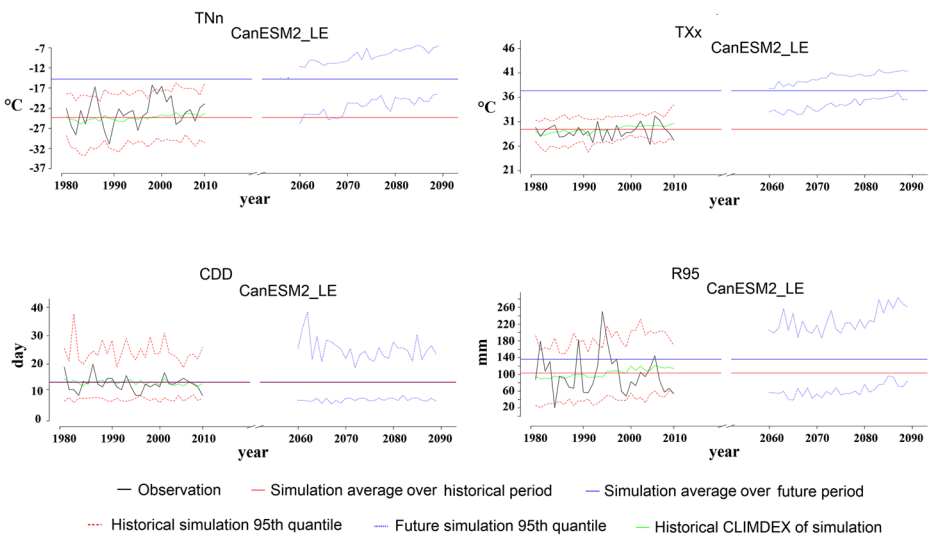


**Fig. 4** Historical (1981–2010) and projected (2060–2089) changes of TNn, TXx, CDD and R95 using gridded observation (solid black line) and CanESM2\_LE. Red and blue dashed lines represent the 95% uncertainty range of the simulations for the historical and future period, respectively. Multi-model ensemble means over the

suggests a reduction in the diurnal range of temperature dominated by daily minimum temperature (Fig. 5). The figure shows the distribution of regional-mean trend over historical and future periods for each ensemble member across four extreme indices. The significant role of daily minimum temperature in the reduction of the diurnal range in the future is consistent with previous studies (Vincent et al. 2018; Vincent and Mekis 2006; Bonsal et al. 2001). The accelerated warming of night-time temperature is associated with feedback effects, presence of clouds, precipitation, soil moisture and the inverse relationship between boundary lateral depth and temperature (Davy et al. 2017; Zhou et al. 2009). In both TNn and TXX, a larger portion of historical trend corresponds to internal variability, whereas this behaviour is reversed in the future period with the external forcing response trend dominating. Precipitation has a relatively large internal variability which is expected as discussed by several other studies (Fischer et al. 2014; Fischer et al. 2013; Deser et al. 2012). Majority of the ensemble members project negative trends in the average consecutive dry days over the study area, although the external forcing response trend is marginally positive in the future period indicating an insignificant trend in the ensemble mean and small forced response in the extreme index. For R95, there is a small positive trend in the ensemble mean but the internal variability component brings a large spatial heterogeneity in the spatial patterns with negative trends dominating the lower part of the basin and high positive trends concentrated in the middle of the basin extending from west to east (Fig. S10).

Figure 6 shows the spatial variation of internal variability and external forcing response in historical and future periods from a single run of CanESM2\_LE for TXX. The figure is generated based on Eq. 1 in which the extreme climate index calculated using the mean of the ensemble is subtracted from the extreme climate index calculated from a single member of the ensemble at each time step across each grid over the entire region. This disassociates the total trend into the two components shown in Fig. 6, highlighting the effect of external forcing response as well as ICV on the trend of the specific extreme index (Dai and Bloecker 2019). The comparison between historical and future periods clearly shows that the trend changes direction across time scales. While in the historical period, the northern part of the study area is dominated by negative residual trends, and positive residual trends in the southern region, the future projection shows a reversal of this pattern with positive trends in the northern region and negative trends in the south. For TNn, while the trend of response to external forcing is quite uniform across the entire region, the residual trend dampens the extremes and produce a slightly positive overall trend in the north and extreme south and negative trends in the middle of the study area in the historical period (Fig. S9). It should be noted that these features are specific to the ensemble member, and every other ensemble member would generate different outcomes while the average over the ensemble would be zero.

The most dominant role of internal variability can be seen in CDD index, where the response to external forcing is quite uniform across the whole region with slightly positive trends; however, internal variability drives the total trend and shows larger increases in the middle region of the study area and negative trends in the south (Fig. 7). In the future period, the residual trend adds to the positive external forcing response in the north and south while dampens the trend in the middle regions. The prevalence of internal variability as the dominating factor in future trends presents a counterpoint to other indices where the footprint of external response is clearly the dominant factor in trends. R95 has a strong negative external forcing response trend across the southern region which is added to by the residual trends while it adds to the trend of extreme precipitation in the central region of the study area (Fig. S10).

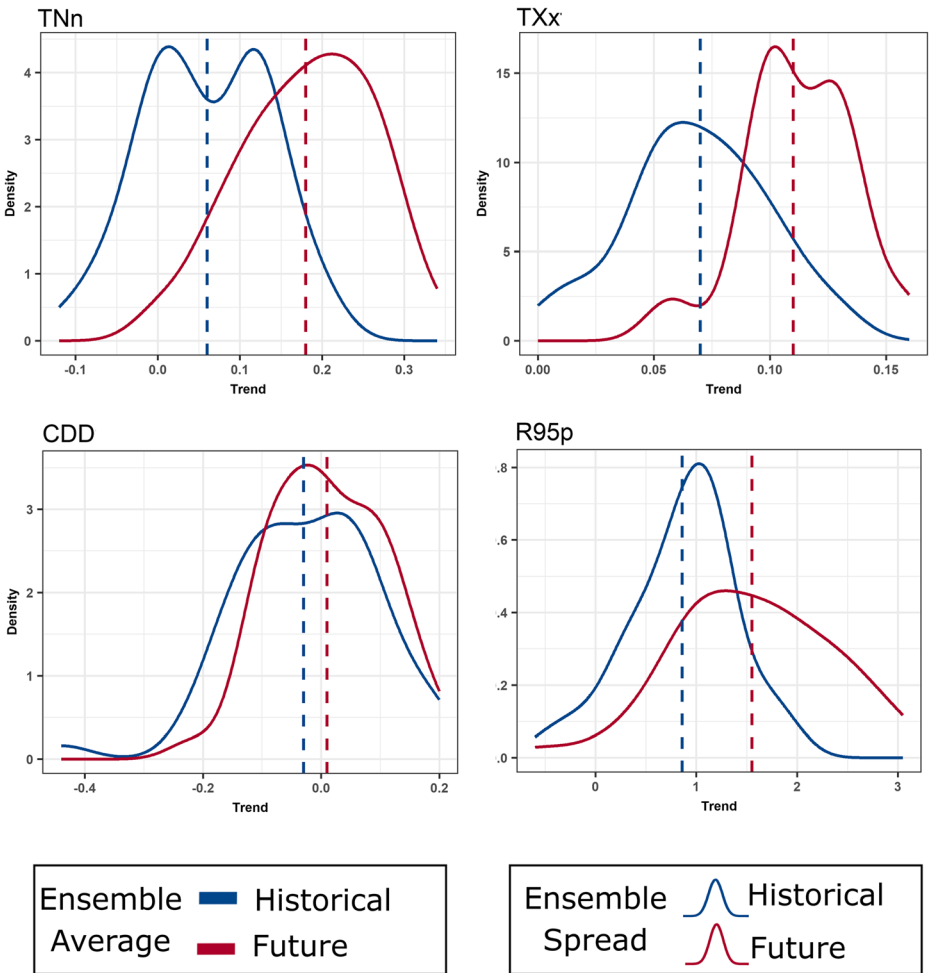


**Fig. 5** Historical and future trends in TNn, TXx, CDD and R95p projected by CanESM2\_LE spatially averaged across the study area. The dotted vertical lines represent the external forcing response trend, while the densities represent the spread of trends from each ensemble member accounting for the internal climate variability

Furthermore, SNR results generated from Eq. 2, (Fig. 8 and S11–S17) reveal that elevation plays a major role in the underlying signal and noise ratio in downscaled precipitation indices. In the high elevation area, along the Rockies, the signal is the dominating factor in the extreme index trends, whereas trends in low elevation areas are noisier. However, in the future period, the signal dominates across the entire region (particularly for temperature-related indices), while remaining strongest in high elevation regions. For TNn and TXx, the historical period is entirely dominated by the underlying noise, while there is a strong signal in the future period (Figs. S16 & S17). Elevation does not show a significant influence on spatial variations of temperature-based index trends. It is also observed that the strength of the signal in the future period is significantly higher for TNn as compared to that for TXx, further confirming that the reduction in the diurnal range of temperature in the future will be dominated by increases in the lower tail of the temperature distribution.

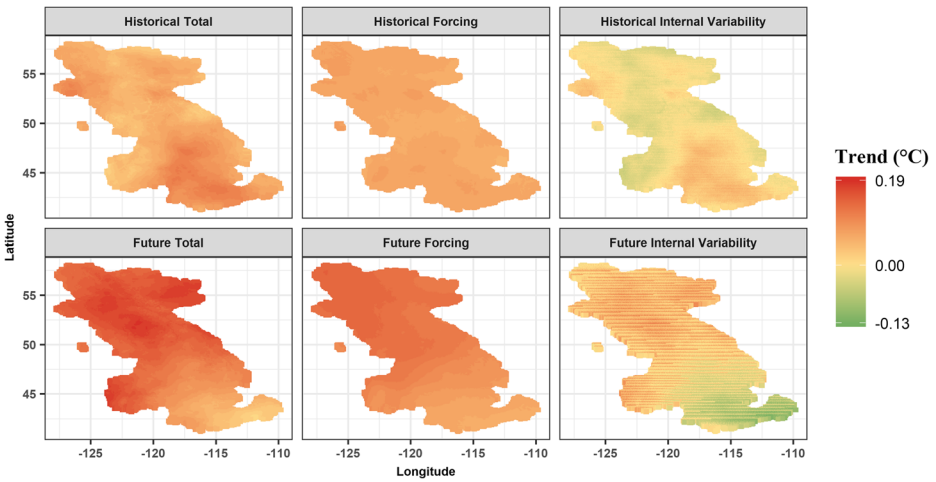


Fig. 6 Contribution of external forcing response and ICV to trends in TXx for the selected ensemble member

### 5 Conclusions

We assess the historical (1981–2010) and future (2060–2089) extreme temperature and precipitation events over four major river basins in northwest North America including Columbia, Fraser, Peace and Campbell with a total area of about 1 M km<sup>2</sup>. Seven GCMs, with different structures and a large ensemble of CanESM2 model simulations (50 members), generated by perturbing its initial conditions, are downscaled to daily temporal and 1/16° spatial resolution using the state-of-the-art BCCAQ-v2 statistical approach.

Overall, downscaled GCM ensembles show increases in the projected frequency and intensity of both dry and wet extremes over the domain. Both ensembles show more extreme hot temperatures and less extreme cold temperatures in the future throughout NWN particularly in higher latitudes and CRB, respectively. Most considerable relative projected changes

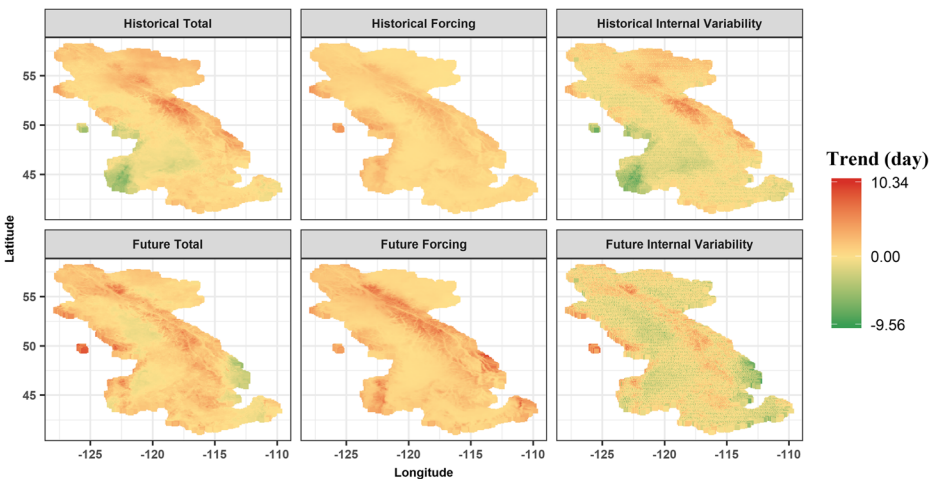
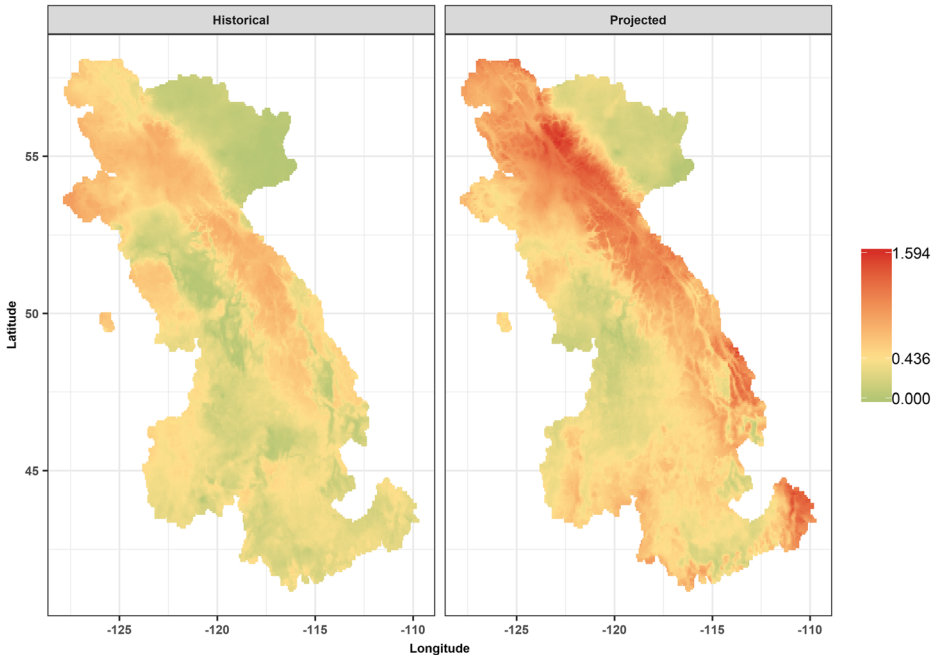


Fig. 7 Spatial variation of trends in CDD external forcing response and internal variability across the study area for an ensemble member

## Spatial variation of absolute Signal to Noise Ratio R95



**Fig. 8** Spatial variation of absolute signal-to-noise ratio (SNR) for R95 for historical (left) and future (right) periods

in CLIMDEX indices are associated with CaRB (indices: CDD, GSL), FRB (TNn, TXx, Rx5day, R95), PRB (TNn, TXx) and CRB (SDII, R95). Tables S1 and S2 show the spatial averages of these projected changes for each river basin using SR\_GCMs and CanESM2\_LE, respectively. Increases in TXx and TNn can impact important industries and economic activities such as fisheries (increase in air temperature and consequently surface water temperature can affect the fish population (Dahlke et al. 2020)) and agriculture in terms of both plants respiration (increase in temperature endangers plant respiration (Ryan 1991) and production (Anderegg et al. 2013)). Moreover, temperature increases are expected to result in more severe and intensified wildfires (Wuebbles et al. 2017), intensify rain-on-snow and snowmelt flooding during winter and spring in this region (Agnihotri and Coulibaly 2020), reduce snowpack (Najafi et al. 2016, 2017a) and consequently the summer streamflow (Najafi et al. 2017b), increase cooling power demand during summer particularly in cities with dense population and cause urban heat island effect (Santamouris et al. 2015). The growing season length is simulated well by both ensembles and projected to increase over the domain particularly over CRB. Furthermore, all precipitation-based indices are projected to increase significantly over the high elevation area. Therefore, NWN is expected to experience more drastic events such as droughts (associated with increased CDD) and floods (due to increases in R10, SDII and R95, and RX5day). The aforementioned changes would directly affect the economy of major cities such as tourism (more intense precipitation adversely affects the tourism (Olya and Alipour 2015)), agriculture (agriculture lands hardly recover from severe droughts (Geng et al. 2015)) and wildfires (due to warm and dry conditions (Herring et al. 2016)).

The results of this study are consistent with previous analyses conducted over the individual river basins, which show overall projected increases in precipitation-based and temperature-

based indices, including FRB (Shrestha et al. 2012), CRB (Rupp et al. 2017), PRB (M. Schnorbus et al. 2011) and CaRB (Mandal et al. 2016). This study provides the first analysis of extreme climate indices using a large ensemble of GCM simulations over NRNA. It also quantifies the role of internal climate variability on the historical and projected trends of CLIMDEX indices at a regional scale.

Models are evaluated using several performance metrics including Taylor diagram and spatial and temporal plots of the ensemble means. Historically, mountainous areas in western and eastern NRNA tend to receive higher rates of precipitation compared to the other regions. Extreme precipitation is projected to be more frequent and intense over these regions including the Coast Mountains, Columbia Mountains and the Rocky Mountains in the future. In addition, the spatial patterns of precipitation-related indices are different from the spatial patterns of temperature-related indices. The ensembles do not capture the number of observed consecutive dry days well, although they project increases over the entire FRB in the future (up to 15 days in a year based on the multi-model ensemble means). In addition, southern and western parts of CRB, which are already dry, are projected to experience more consecutive dry days. The role of internal variability in projected trends of the extremes is also explored. It is found that internal variability plays a more significant role in precipitation trends as compared to temperature. While considering the response to external forcing alone, precipitation extremes have a positive trend throughout the basin and the trends become more spatially distinct when internal variability is accounted for with significant positive trends in the middle of the study area and negative trends in the south. The results also show how internal variability can overwhelm the forced response locally within the basin as is evident from the spatial patterns of trends in the response to external forcing and residual trends. Based on the SNR analyses, higher elevations show stronger forcing signals for precipitation-based indices compared to other regions of NRNA. The trends for CDD, however, are insignificant as internal forcing plays the dominant role rather than the response to external forcing.

The results of this study, based on a large suite of downscaled and bias-corrected GCM simulations, show that NRNA will experience more severe extremes under the RCP 8.5 emission scenario. This can put more than 14 million people living in this region, as well as its ecosystem, socioeconomic activities and infrastructure, at risk, which necessitates the development of effective adaptation strategies.

**Supplementary Information** The online version contains supplementary material available at <https://doi.org/10.1007/s10584-021-03037-9>.

**Acknowledgements** We would like to thank James Hiebert and Arelia Werner for their support in downscaling using BCCAQ2.

**Funding** The funding for this project is provided by the NSERC Discovery grant.

## References

Abbasian MS, Najafi MR, Abrishamchi A (2020a) Increasing risk of meteorological drought in the Lake Urmia basin under climate change: introducing the precipitation–temperature deciles index. *J Hydrol* 592:125586. <https://doi.org/10.1016/j.jhydrol.2020.125586>



- Abbasian MS, Najafi MR, Abrishamchi A (2020b) Increasing risk of meteorological drought in the Lake Urmia basin under climate change: introducing the precipitation–temperature deciles index. *J Hydrol* 592:125586. <https://doi.org/10.1016/j.jhydrol.2020.125586>
- Acero FJ, García JA, Gallego MC (2011) Peaks-over-threshold study of trends in extreme rainfall over the Iberian Peninsula. *J Clim* 24(4):1089–1105. <https://doi.org/10.1175/2010JCLI3627.1>
- Agnihotri J, Coulibaly P (2020) Evaluation of snowmelt estimation techniques for enhanced spring peak flow prediction. *Water* 12(5):1290. <https://doi.org/10.3390/w12051290>
- Anderegg WRL, Kane JM, Anderegg LDL (2013, January 9) Consequences of widespread tree mortality triggered by drought and temperature stress. *Nat Clim Chang* 3:30–36. <https://doi.org/10.1038/nclimate1635>
- Andrishak R, Hicks F (2008) Impact of climate change on the peace river thermal ice regime. In: Cold region atmospheric and hydrologic studies. The Mackenzie GEWEX experience, vol 2, pp 327–343. [https://doi.org/10.1007/978-3-540-75136-6\\_17](https://doi.org/10.1007/978-3-540-75136-6_17)
- Bennett KE, Werner AT, Schnorbus M (2012) Uncertainties in hydrologic and climate change impact analyses in headwater basins of British Columbia. *J Clim* 25(17):5711–5730. <https://doi.org/10.1175/JCLI-D-11-00417.1>
- Bi D, Dix M, Marsland SJ, O’Farrell S, Rashid H, Uotila P, Hirst AC, Kowalczyk E, Golebiewski M, Sullivan A, Yan H (2013) The ACCESS coupled model: description, control climate and evaluation. *Aust Meteorol Oceanogr J* 63(1):41–64
- Bonsal BR, Zhang X, Vincent LA, Hogg WD (2001) Characteristics of daily and extreme temperatures over Canada. *J Clim* 14(9):1959–1976
- Bürger G et al (2013) Downscaling extremes: an intercomparison of multiple methods for future climate. *J Clim* 26(10):3429–3449. <https://doi.org/10.1175/JCLI-D-12-00249.1>
- Bush E, Lemmen DS (2019) ‘Canada’s changing climate report’, Government of Canada: Ottawa, ON, Canada, p 444. Available at: <https://www.nrcan.gc.ca/environment/impacts-adaptation/21177>
- Chen H, Xu CY, Guo S (2012) Comparison and evaluation of multiple GCMs, statistical downscaling and hydrological models in the study of climate change impacts on runoff. *J Hydrol* 434–435:36–45. <https://doi.org/10.1016/j.jhydrol.2012.02.040>
- Chylek P, Li J, Dubey MK, Wang M, Lesins G (2011) Observed and model simulated 20th century Arctic temperature variability: Canadian earth system model CanESM2. *Atmospheric Chemistry and Physics Discussions* 11(8):22893–22907
- Dahlke FT, Wohlrab S, Butzin M, Pörtner HO (2020) Thermal bottlenecks in the life cycle define climate vulnerability of fish. *Science (New York, N.Y.)* 369(6499):65–70. <https://doi.org/10.1126/science.aaz3658>
- Dai A, Bloecker CE (2019) Impacts of internal variability on temperature and precipitation trends in large ensemble simulations by two climate models. *Clim Dyn* 52(1–2):289–306. <https://doi.org/10.1007/s00382-018-4132-4>
- Davy R, Esau I, Chernokulsky A, Outten S, Zilitinkevich S (2017) Diurnal asymmetry to the observed global warming. *Int J Climatol* 37(1):79–93
- Deser C, Knutti R, Solomon S, Phillips AS (2012) Communication of the role of natural variability in future North American climate. *Nat Clim Chang* 2(11):775–779. <https://doi.org/10.1038/nclimate1562>
- Diaz-Nieto J, Wilby RL (2005) A comparison of statistical downscaling and climate change factor methods: impacts on low flows in the river Thames, United Kingdom. *Clim Chang* 69(2–3):245–268. <https://doi.org/10.1007/s10584-005-1157-6>
- Fauzi F, Kuswanto H, Atok RM (2020) Bias correction and statistical downscaling of earth system models using quantile delta mapping (QDM) and bias correction constructed analogues with quantile mapping reordering (BCCAQ). *J Phys Conf Ser* 1538(1):12050. <https://doi.org/10.1088/1742-6596/1538/1/012050>
- Field CB et al (2014) Cambio climático 2014 Impactos, adaptación y vulnerabilidad Edición a cargo de Editores científicos para la traducción. Available at: [www.ipcc.ch](http://www.ipcc.ch). ()
- Fischer E, Beyerle U, Knutti R (2013) Robust spatially aggregated projections of climate extremes. *Nat Clim Chang* 3(12):1033–1038
- Fischer E, Sedláček J, Hawkins E, Knutti R (2014) Models agree on forced response pattern of precipitation and temperature extremes. *Geophys Res Lett* 41(23):8554–8562
- Frich P et al (2002) Observed coherent changes in climatic extremes during the second half of the twentieth century. *Clim Res* 19(3):193–212. <https://doi.org/10.3354/cr019193>
- Geng S, Yan D, Zhang T, Weng B, Zhang ZB (2015) Effects of drought stress on agriculture soil. *Nat Hazards* Retrieved from. <https://doi.org/10.1007/s11069-014-1409-8.pdf>
- Gent PR, Danabasoglu G, Donner LJ, Holland MM, Hunke EC, Jayne SR, Lawrence DM, Neale RB, Rasch PJ, Vertenstein M, Worley PH (2011) The community climate system model version 4. *J Clim* 24(19):4973–4991
- Giorgetta MA, Jungclaus J, Reick CH, Legutke S, Bader J, Böttinger M, Brovkin V, Crueger T, Esch M, Fieg K, Glushak K (2013) Climate and carbon cycle changes from 1850 to 2100 in MPI-ESM simulations for the Coupled Model Intercomparison Project phase 5. *Journal of Advances in Modeling Earth Systems* 5(3):572–597

- Hansen J, Sato M, Ruedy R, Lo K, Lea DW, Medina-Elizade M (2006) Global temperature change. *Proc Natl Acad Sci U S A* 103(39):14288–14293. <https://doi.org/10.1073/pnas.0606291103>
- Hegerl GC, Black E, Allan RP, Ingram WJ, Polson D, Trenberth KE, ..., Zhang X (2015) Challenges in quantifying changes in the global water cycle. *Bull Am Meteorol Soc* 96:1097–1115. <https://doi.org/10.1175/BAMS-D-13-00212.1>
- Herring SC, Hoell A, Hoerling MP, J. P. K, Schreck CJ III, P. A. S (2016) Explaining extreme events of 2015 from a climate perspective. *Am Meteorol Soc*. <https://doi.org/10.1175/BAMS-D-16-0149>
- Hidalgo HG, Dettinger MD, Cayan DR (2008) Downscaling with constructed analogues: daily precipitation and temperature fields over the United States California energy commission pier final project report. California energy commission pier final project report. CEC-500-2007-123
- Hunter RD et al (2005) Climatologically aided mapping of daily precipitation and temperature. *J Appl Meteorol* 44(10):1501–1510. <https://doi.org/10.1175/JAM2295.1>
- Jalili Pirani F, Najafi MR (2020) Recent trends in individual and multivariate compound flood drivers in Canada's coasts. *Water Resources Research* 56(8):e2020WR027785
- Jones C, Hughes JK, Bellouin N, Hardiman SC, Jones GS, Knight J, Liddicoat S, O'connor FM, Andres RJ, Bell C, Boo KO (2011) The HadGEM2-ES implementation of CMIP5 centennial simulations. *Geoscientific Model Development* 4:543–570
- Karl TR, Nicholls N, Ghazi A (1999) 'CLIVAR/GCOS/WMO workshop on indices and indicators for climate extremes - workshop summary', *Climatic Change*. Springer-Verlag London Ltd, 42(1):3–7. <https://doi.org/10.1023/A:1005491526870>
- Kharin VV, Zwiers FW, Zhang X, Hegerl GC (2007) Changes in temperature and precipitation extremes in the IPCC Ensemble of Global Coupled Model Simulations. *J Clim* 20(8):1419–1444. <https://doi.org/10.1175/JCLI4066.1>
- Kiktev D et al (2003) Comparison of modeled and observed trends in indices of daily climate extremes. *J Clim* 16(22):3560–3571. [https://doi.org/10.1175/1520-0442\(2003\)016<3560:COMAOT>2.0.CO;2](https://doi.org/10.1175/1520-0442(2003)016<3560:COMAOT>2.0.CO;2)
- Krasting JP et al (2013) Future changes in northern hemisphere snowfall. *J Clim* 26(20):7813–7828. <https://doi.org/10.1175/JCLI-D-12-00832.1>
- Li G et al (2018) Indices of Canada's future climate for general and agricultural adaptation applications. *Clim Chang* 148(1–2):249–263. <https://doi.org/10.1007/s10584-018-2199-x>
- Mandal S, Srivastav RK, Simonovic SP (2016) Use of beta regression for statistical downscaling of precipitation in the Campbell River basin, British Columbia, Canada. *Journal of Hydrology*. Elsevier 538:49–62. <https://doi.org/10.1016/J.JHYDROL.2016.04.009>
- Maurer EP et al (2010) The utility of daily large-scale climate data in the assessment of climate change impacts on daily streamflow in California. *Hydrol Earth Syst Sci* 14(6):1125–1138. <https://doi.org/10.5194/hess-14-1125-2010>
- Morrison J, Quick MC, Foreman MGG (2002) Climate change in the Fraser River watershed: flow and temperature projections. *J Hydrol* 263(1–4):230–244. [https://doi.org/10.1016/S0022-1694\(02\)00065-3](https://doi.org/10.1016/S0022-1694(02)00065-3)
- Murdoch TQ et al (2013) Climate change and extremes in the Canadian Columbia Basin. <https://doi.org/10.1080/0705590.2013.816932>
- Najafi MR, Moradkhani H, Wherry SA (2011) Statistical downscaling of precipitation using machine learning with optimal predictor selection. *J Hydrol Eng* 16(8):650–664. [https://doi.org/10.1061/\(ASCE\)HE.1943-5584.0000355](https://doi.org/10.1061/(ASCE)HE.1943-5584.0000355)
- Najafi MR, Zwiers FW, Gillett NP (2016) Attribution of the spring snow cover extent decline in the Northern Hemisphere, Eurasia and North America to anthropogenic influence. *Clim Chang* 136(3–4):571–586. <https://doi.org/10.1007/s10584-016-1632-2>
- Najafi MR, Zwiers F, Gillett N (2017a) Attribution of the observed spring snowpack decline in British Columbia to anthropogenic climate change. *J Clim* 30(11):4113–4130. <https://doi.org/10.1175/JCLI-D-16-0189.1>
- Najafi MR, Zwiers FW, Gillett NP (2017b) Attribution of observed streamflow changes in key British Columbia drainage basins. *Geophys Res Lett* 44(21):11,012–11,020. <https://doi.org/10.1002/2017GL075016>
- Northcote TG (1996) Effects of human population growth on the Fraser and Okanagan River systems, Canada: a comparative inquiry. *GeoJournal* 40(1–2):127–133. <https://doi.org/10.1007/BF00222538>
- Olya HGT, Alipour H (2015) Risk assessment of precipitation and the tourism climate index. *Tour Manag* 50: 73–80. <https://doi.org/10.1016/j.tourman.2015.01.010>
- Orlowsky B, Seneviratne SI (2012) Global changes in extreme events: regional and seasonal dimension. *Clim Chang* 110(3–4):669–696. <https://doi.org/10.1007/s10584-011-0122-9>
- Pal JS, Giorgi F, Bi X (2004) Consistency of recent European summer precipitation trends and extremes with future regional climate projections. *Geophys Res Lett* 31(13). <https://doi.org/10.1029/2004GL019836>
- Pulwarty RS, Redmond KT (1997) Climate and salmon restoration in the Columbia River basin: the role and usability of seasonal forecasts. *Bulletin of the American Meteorological Society*. American Meteorological Society 78(3):381–397. [https://doi.org/10.1175/1520-0477\(1997\)078<0381:CASRIT>2.0.CO;2](https://doi.org/10.1175/1520-0477(1997)078<0381:CASRIT>2.0.CO;2)

- Rupp DE, Abatzoglou JT, Mote PW (2017) Projections of 21st century climate of the Columbia River Basin. 49: 1783–1799. <https://doi.org/10.1007/s00382-016-3418-7>
- Ryan MG (1991) Effects of climate change on plant respiration. *Ecol Appl* 1(2):157–167. <https://doi.org/10.2307/1941808>
- Santamouris M, Cartalis C, Synnefa A, Kolokotsa D (2015) On the impact of urban heat island and global warming on the power demand and electricity consumption of buildings - a review. *Energy and Buildings* 98:119–124. <https://doi.org/10.1016/j.enbuild.2014.09.052>
- Schnorbus M, Werner AT, Shrestha R (2011) Impact of projected climate change within two hydrologic regimes in British Columbia, Canada. *AGUFM 2011:H13C-1228*
- Shrestha RR, Schnorbus MA, Werner AT, Berland AJ (2012) Modelling spatial and temporal variability of hydrologic impacts of climate change in the Fraser River basin, British Columbia, Canada. *Hydrol Process* 26(12):1840–1860. <https://doi.org/10.1002/hyp.9283>
- Sillmann J, Roeckner E (2008) Indices for extreme events in projections of anthropogenic climate change. *Clim Chang* 86(1–2):83–104. <https://doi.org/10.1007/s10584-007-9308-6>
- Sillmann J et al (2013) Climate extremes indices in the CMIP5 multimodel ensemble: part 2. Future climate projections. *Journal of Geophysical Research: Atmospheres*. John Wiley & Sons, Ltd 118(6):2473–2493. <https://doi.org/10.1002/jgrd.50188>
- Singh H, Najafi MR (2020) Evaluation of gridded climate datasets over Canada using univariate and bivariate approaches: implications for hydrological modelling. *J Hydrol* 584:124673
- Singh H, Pirani FJ, Najafi MR (2020) Characterizing the temperature and precipitation covariability over Canada. *Theor Appl Climatol* 139(3–4):1543–1558. <https://doi.org/10.1007/s00704-019-03062-w>
- Singh H, Najafi MR, Cannon AJ (2021) Characterizing non-stationary compound extreme events in a changing climate based on large-ensemble climate simulations. *Clim Dyn*. <https://doi.org/10.1007/s00382-020-05538-2>
- Tebaldi C et al (2006) Going to the extremes. *Climatic Change*. Kluwer Academic Publishers 79(3–4):185–211. <https://doi.org/10.1007/s10584-006-9051-4>
- Vincent LA, Mekis E (2006) Changes in daily and extreme temperature and precipitation indices for Canada over the twentieth century. *Atmosphere-Ocean* 44(2):177–193
- Vincent LA, Zhang X, Mekis É, Wan H, Bush EJ (2018) Changes in Canada's climate: trends in indices based on daily temperature and precipitation data. *Atmosphere-Ocean* 56(5):332–349
- Voldoire, A., Sanchez-Gomez, E., y Méliá, D.S., Decharme, B., Cassou, C., Sénési, S., Valcke, S., Beau, I., Alias, A., Chevallier, M. and Déqué, M., 2013. The CNRM-CM5. 1 global climate model: description and basic evaluation. *Clim Dyn*, 40(9–10), pp.2091–2121
- Werner AT, Cannon AJ (2016) Hydrologic extremes - an intercomparison of multiple gridded statistical downscaling methods. *Hydrol Earth Syst Sci* 20(4):1483–1508. <https://doi.org/10.5194/hess-20-1483-2016>
- Werner A et al (2019) 'A long-term, temporally consistent, gridded daily meteorological dataset for northwestern North America', *nature.com*. Available at: <https://www.nature.com/articles/sdata2018299> ()
- Whan K, Zwiers F (2016) Evaluation of extreme rainfall and temperature over North America in CanRCM4 and CRCM5. *Clim Dyn* 46. <https://doi.org/10.1007/s00382-015-2807-7>
- Wuebbles D, Fahey D, Hibbard K (2017) 'Climate science special report: fourth national climate assessment, volume I'. Available at: [https://repository.library.noaa.gov/view/noaa/19486/noaa\\_19486\\_DS1.pdf](https://repository.library.noaa.gov/view/noaa/19486/noaa_19486_DS1.pdf) ()
- Xie S-P, Deser C, Vecchi GA, Collins M, Delworth TL, Hall A, ... Watanabe M (2015) Towards predictive understanding of regional climate change. <https://doi.org/10.1038/NCLIMATE2689>
- Yang Y, Tang J, Xiong Z, Wang S, Yuan J (2019) An intercomparison of multiple statistical downscaling methods for daily precipitation and temperature over China: present climate evaluations. *Clim Dyn* 53(7–8): 4629–4649. <https://doi.org/10.1007/s00382-019-04809-x>
- Zhang Y, Najafi MR (2020) Probabilistic numerical modeling of compound flooding caused by tropical storm Matthew over a data-scarce coastal environment. *Water Resources Research* 56(10):e2020WR028565
- Zhang X et al (2005) Avoiding inhomogeneity in percentile-based indices of temperature extremes. *J Clim* 18(11):1641–1651. <https://doi.org/10.1175/JCLI3366.1>
- Zhang X et al (2011) Indices for monitoring changes in extremes based on daily temperature and precipitation data. *Wiley Interdiscip Rev Clim Chang* 2(6):851–870. <https://doi.org/10.1002/wcc.147>
- Zhou L, Dai Y, Vose RS, Zou C-Z, Tian Y, Chen H (2009) Spatial dependence of diurnal temperature range trends on precipitation from 1950 to 2004. *Clim Dyn* 32:429–440